Enhanced Emission from Interlayer Excitons Coupled to Plasmonic Gap Cavities

Enhanced Emission from Interlayer Excitons Coupled to Plasmonics Gap Cavities

Thinh N. Tran[1], Sejeong Kim[2], Simon J. U. White[1], Minh Anh Phan Nguyen[1], Licheng Xiao[3,4], Stefan Strauf[3,4], Tieshan Yang[1,5], Igor Aharonovich[1,5*] and Zai-Quan Xu[1*]

[1]School of Mathematical and Physical Sciences, University of Technology Sydney, Ultimo, New South Wales 2007, Australia

[2]Department of Electrical and Electronic Engineering, Faculty of Engineering and Information Technology, University of Melbourne, Victoria 3010, Australia

[3]Department of Physics, Stevens Institute of Technology, Hoboken, New Jersey 07030, USA

[4]Center for Quantum Science and Engineering, Stevens Institute of Technology, Hoboken, New Jersey 07030, USA

[5]ARC Centre of Excellence for Transformative Meta-Optical Systems (TMOS), University of Technology Sydney, Ultimo, New South Wales 2007, Australia

*Corresponding Authors

E-mail: igor.aharonovich@uts.edu.au and zaiquan.xu@uts.edu.au.

KEYWORDS: transition metal dichalcogenide, heterostructures, interlayer excitons, plasmonic gap cavities.

Abstract

The emergence of interlayer excitons from atomic layered transition metal dichalcogenides (TMDCs) heterostructures has drawn tremendous attention due to their unique and exotic optoelectronic

properties. Coupling the IEs into optical cavities provides distinctive electromagnetic environments which plays an important role in controlling multiple optical processes such as optical nonlinear generation or photoluminescence (PL) enhancement. Here, we report the integration of interlayer excitons in TMDCs into plasmonic nanocavities based on a nanocube on a metallic mirror. Spectroscopic studies reveal an order of magnitude enhancement of the interlayer exciton at room temperature and a 5-time enhancement in fluorescence at cryogenic temperatures. Cavity modelling reveal the enhancement of the emission is attributed to both increased excitation efficiency and Purcell effect from the cavity. Our results show a novel method to control the excitonic processes in TMDC heterostructures to build high performance photonics and optoelectronics devices.

Introduction

Interlayer excitons (IEs) in van der Waals (vdW) heterostructures emerged as a promising platform for the studies of excitonic phenomena, many body physics, and optoelectronics.[1-4] The IEs are constituted electron-hole pairs donated from adjacent monolayers, forming an indirect system with spatially separated but bound electron-hole pairs via Coulomb interactions[5-7] (**Figure 1a**). When two monolayer transition metal di-chalcogenide (TMDCs) crystals are in close contact and form a type II band structure alignment, IEs will form due to the ultrafast charge transfer between the monolayers.[8, 9] As a result, the formation of the IEs would lead to a quench of the photoluminescence (PL) emission intensity of the individual monolayers. The emission energy from IEs is lower than the individual monolayers and the intensity is highly dependent on the stacking angles.[10-13]

The recent development of the 2D materials family and the alignment transfer technique have enabled the birth of a plethora of IEs with novel physical properties which hold a great potential for chip-integrated optoelectronics applications.[14-20] For example, the IEs are fascinating platform for study many-body effects, such as Bose–Einstein condensation and superfluidity[21, 22]. Moreover, the moiré pattern that arises due to the lattice mismatch and rotation angle between the adjacent layers, leading to the moiré interlayer excitons, which open the door for manipulation[17] of quasi-particles towards quantum information systems.

The electric dipole from IEs is out-of-plane, which suggests the quantum efficiency of IEs is typically low.[2, 23, 24] During the past few years, there have been several strategies to enhance the emission intensity of IEs to obtain deep insight into physical properties of IEs by optimizing the excitation, emission and collections. For example, TMDs[25] and their IEs have been coupled into dielectric cavities, such as microdisk cavities[26], 2D photonic crystals[27, 28] and Mie resonators[29] for enhanced

emission and lasing at room temperatures.[30, 31] However, it is often challenging to spectrally match the IEs to high optical quality factor dielectric cavity modes. Additionally, placing the inhomogeneous materials at top of dielectric cavities will deteriorate their optical performance.[32]

Here, we report on the integration of IEs from a heterostructures of tungsten di-sulphide and molybdenum di-sulphide (WS_2/MoS_2), into a nanoparticle-on-mirror plasmonic gap cavity. We demonstrate over an order of magnitude enhancement in PL intensity when IEs resonate with the plasmonic structures at room temperature. We further performed optical measurements at cryogenic temperatures (5 K) and observed a 5-times enhancement in PL intensity together with lifetime reduction in both fast and slow decay channels. The finite-difference time-domain (FDTD) simulation results reveal the enhancement of the emission is attributed to the higher excitation efficiency from the cavity accompanied with a Purcell enhancement. Our results present a novel approach to improve the excitonic processes in IEs from TMDCs heterojunctions and shed light on IEs based photonics and optoelectronic devices in near future.

Results and Discussions

We chose a nanoplasmonic gap cavity, consisting of a silver nanocube (~100 nm edge length) and an ultraflat gold mirror (~90 nm thickness).[33-36] The resonance from these plasmonic gap cavities is broadband and thus is easily matched to the emission from IEs. It is expected that this type of cavities would enhance the emission from both in-plane and out-of-plane emitting dipoles by accelerating the emission cycles (Purcell effect) and/or redirect the radiation pattern to favour collection. A schematic illustration of the nanogap cavity integrated IEs is presented in **Figure 1b**.

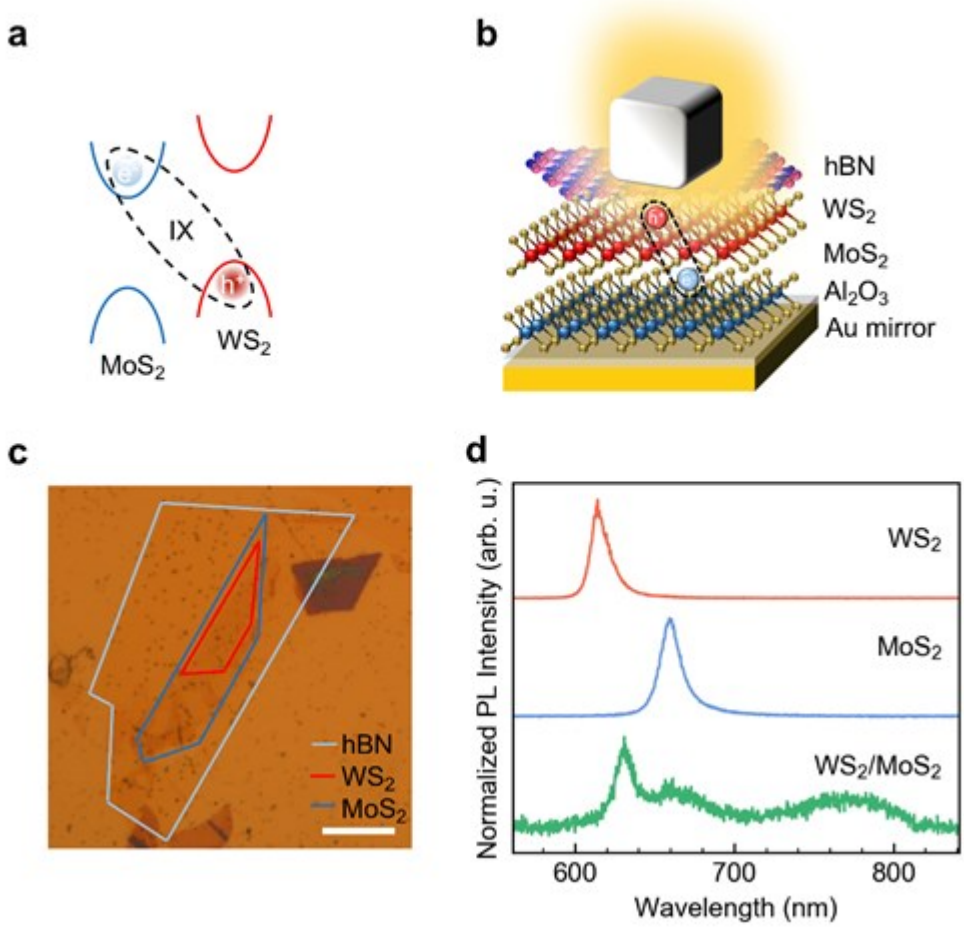

Figure 1. *WS_2/MoS_2 heterostructure integrates with a plasmonic gap cavity. (a) Schematic of the type II band alignment of a WS_2/MoS_2 heterostructure. (b) 3D illustration WS_2/MoS_2 heterostructure integrates with a plasmonic gap cavity. The gap cavity consists of a 100 nm silver nanocube and an ultra-flat gold film. The gold film is coated with 3nm thick Al_2O_3. A thin hBN flake is inserted as a space to tune the resonance wavelength to match the interlayer emission. (c) An optical image of the WS_2/MoS_2 heterostructure in the plasmonic cavity (scale bar: 5 μm), individual 2D flakes are outlined for clarity. (d) Normalized photoluminescence spectra of isolated monolayers WS_2 (red), MoS_2 (blue) and IEs (green, off cavity) at room temperature. The samples were excited with a 200 μW 532nm continuous wave laser.*

The samples were fabricated using tape-exfoliated monolayer WS_2 and MoS_2. These crystals were deterministically aligned and stacked using a pick-and-place method before being released to the gold substrates. A thin layer of hexagonal boron nitride (hBN) flake (<10 nm) was used as a stamp. The silver nanocubes were diluted and dropped onto the heterostructures to form the nanogap modes. An optical microscope image is shown in **Figure 1c** with the individual crystals outlined in different

colours (red: WS_2, blue: MoS_2 and grey: hBN) for clarity. The relative crystal orientation between WS_2 and MoS_2 were aligned with a precision ~ 1° along their longer edges. The normalised PL spectra from monolayer WS_2, MoS_2 and IEs are plotted in **Figure 1d**. The peaks centred at ~ 620 nm (red) [37] and ~ 660 nm (blue)[38] are associated with excitonic emission from WS_2 and MoS_2 monolayers, respectively. Some of the peaks rise at the longer wavelength are might be intralyer excitons and the formation are highly determined by multifactor, such as stacking angle, strain and materials combinations.[39] The significantly reduced intensity from these two peaks together with the rise of the peak at ~ 780 nm indicates the successful formation of IEs according to the literature. [5, 29, 40].

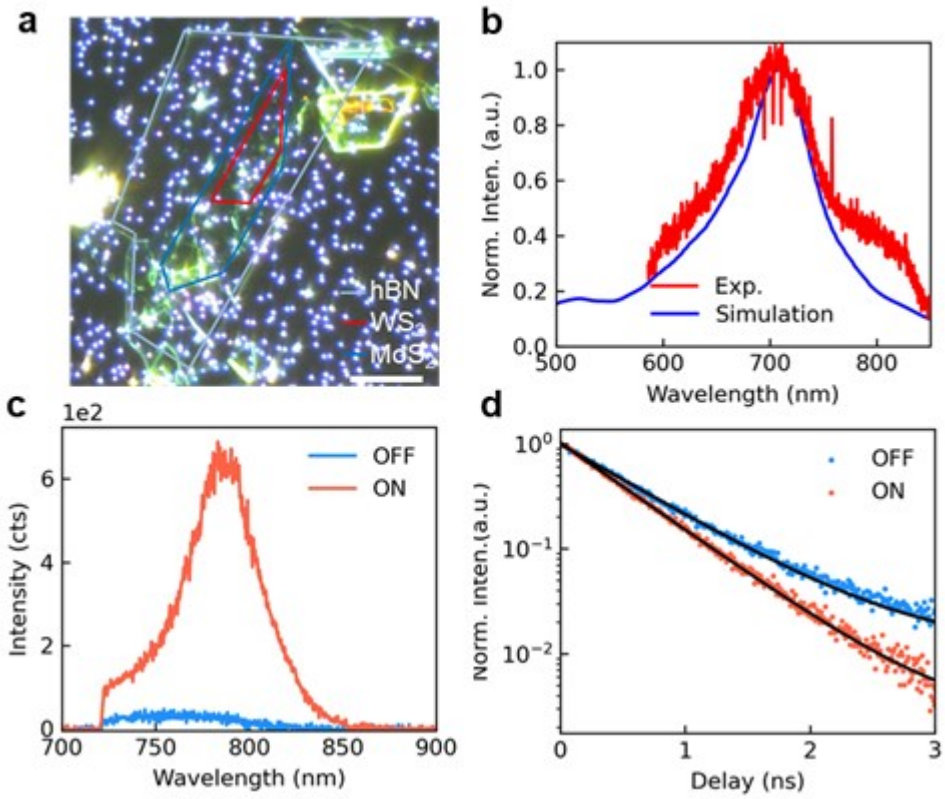

Figure 2. *(a) Dark-field image of corresponding overlapped region shown in Figure 1c. The 2D flakes are outlined and individual silver nanocubes are resolved. Scale bar: 5 μm. (b) Experimental and simulated optical scattering of a single nanocavity. (c) PL comparison between cavity coupling IE (red) and non-coupling IE (blue). (d) Time resolved PL of cavity coupled IE (red) and intrinsic IE (blue). The curves were fitted with a single exponential (black). The extracted lifetimes from fast decay are 526 ps and 652 ps, respectively.*

Systematic studies were performed to compare the emission of the IEs on and off plasmonic gap cavity. **Figure 2a** presents the dark-field image collected from the same sample region as shown in **Figure 1c**. The shining spots correspond to the silver nanocubes. There are ~15 cubes on top of the heterostructure regions, providing enough sample spots to compare the performance of the IEs coupled into cavities. The scattering spectra were collected from the cubes while shining halogen light on the sample with an incident angle of 28°.[41] The normalised spectrum is shown in **Figure 2b**. The spectrum spans from 580 to 820 nm with a peak maximum centred at ~ 700 nm. The simulated scattering spectrum is also plotted which overlaps well with the experimental data. There is also a slight enhancement at ~532 nm which is not seen in the experimental results as it is blocked by our dichroic filter.

The PL spectra from the sample were then collected from the pristine IEs and cavity coupled ones, as shown in **Figure 2c.** The PL from pristine IEs (red) shows maximum intensity at 765 nm, while the cavity-coupled IEs (blue) is red-shifted to ~780 nm, probably due to the cavity resonance. An overall ~ 15-times enhancement in peak height is observed, indicating that the plasmonic cavity has significantly enhanced the excitonic emission of IEs. Time-resolved PL (TRPL) measurements were then performed to understand the results. **Figure 2d** shows the TRPL measurements from pristine (red) and cavity coupled IEs (blue), as well as the instrument response function (IRF). The experimental decay curves were fitted using a double-exponential function. The lifetimes extracted from fast decay channels are 526 ps and 652 ps, respectively, corresponding to a measured reduction of 20%. The absolute lifetime values were longer than the ones reported before[5], probably because our samples have lower non-radiative decay rate at ambient conditions.

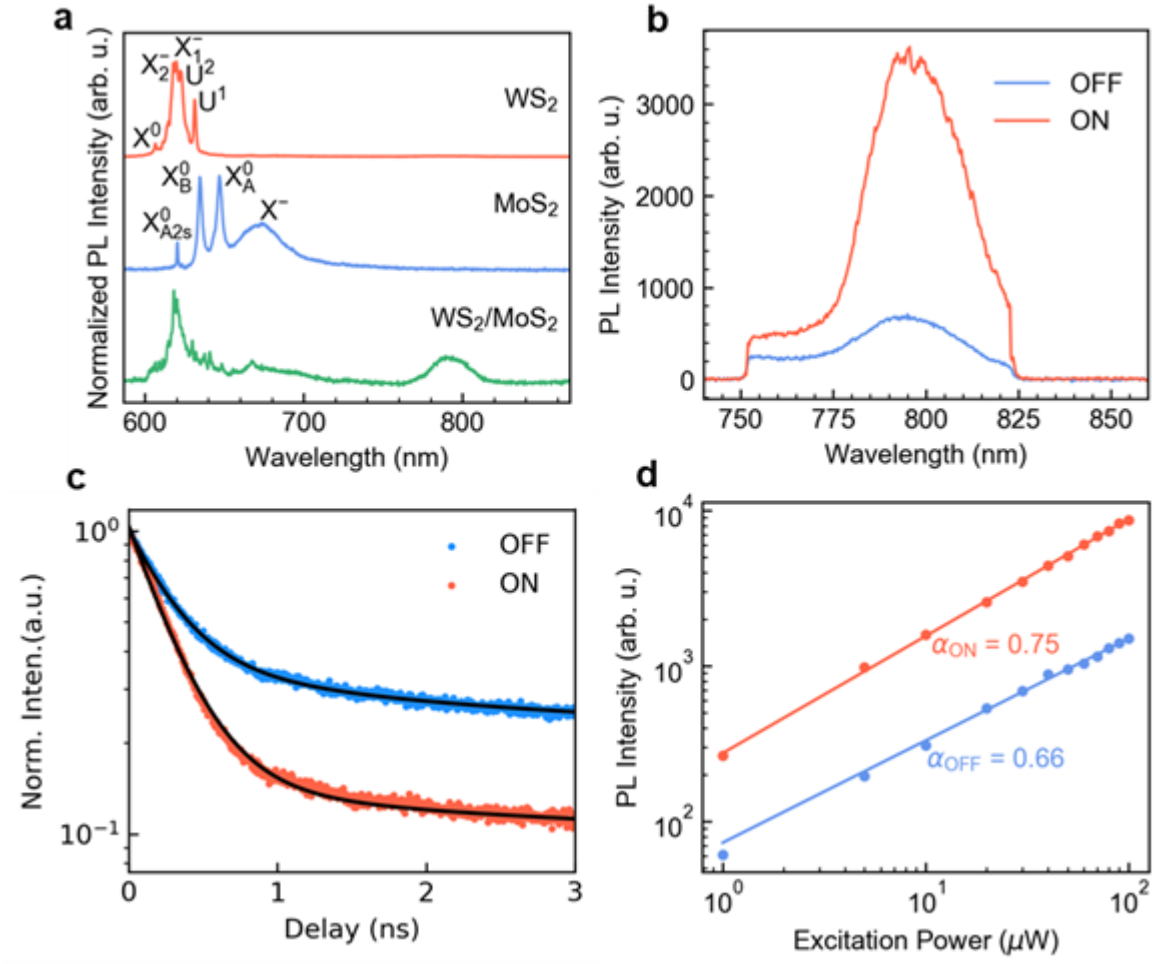

Figure 3. *Plasmonic nanocavity coupling of the interlayer exciton at 5 K. (a) PL spectra of isolated monolayers WS_2(red), MoS_2 (blue) and IEs (green) at 5 K. (b) Interlayer exciton PL comparison between on (red) and off (blue) plasmonic nanocavity. PL intensity increases about 5 times in the coupling region. (c) Time resolved PL shows the reduction in longed-lived IE in both fast and slow decay channels. (d) The PL intensity as the function of excitation power is fitted by a power law (P^{α}) with the critical exponents α.*

We continued to study the system at cryogenic temperatures. The normalised PL spectra at 5K from monolayer WS_2, MoS_2 and IEs are plotted in **Figure 3a**. A narrower excitonic emission from the WS_2 and the MoS_2 monolayers are clearly visible. Comparing the PL emission from IEs on and off cavity, as shown in **Figure 3b**, a 5-time enhancement of the coupled system is observed. **Figure 3c** shows the decay rates of the pristine and cavity coupled IEs emission. The experimental data are fit using a double exponential, with fast / slow decay constants extracted to be 263 ps / 343 ps and 2.29 ns / 3.09 ns for the coupled and non-coupled systems, respectively[6, 23, 42]. The time resolved measurements

demonstrate reduction in fast and slow decay channels from IEs to be about 23.3% and 25.8%, respectively. The lifetime reduction at cryogenic temperatures is on part with the change observed at room temperature, consistent with the plasmonic cavities. Finally, **figure 3d** presents the PL intensity of an IE as a function of excitation power for the cavity coupled (red) and pristine system (blue). As expected for the excitonic system, no saturation is observed.

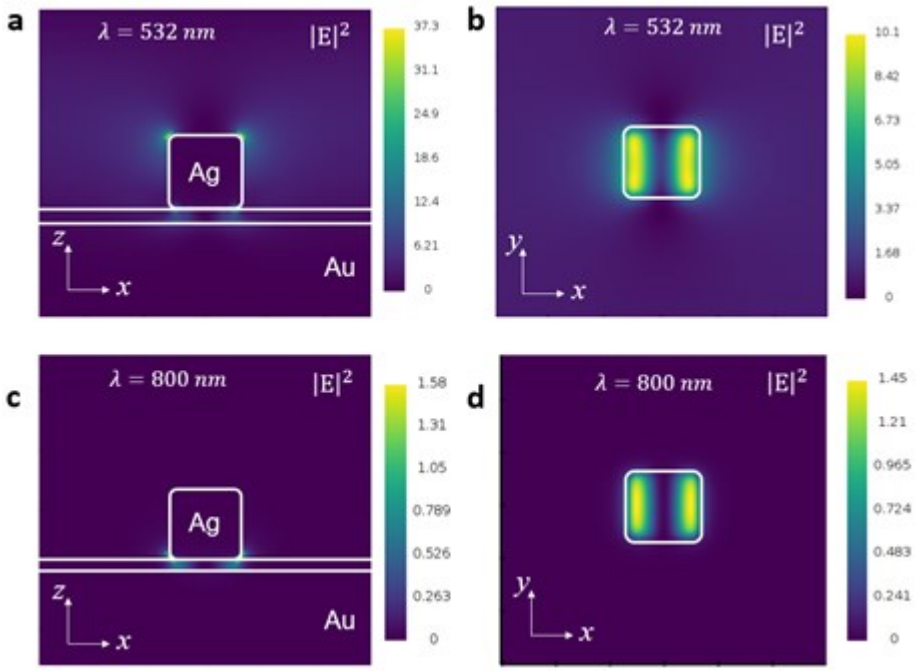

Figure 4. *FDTD simulation results of the gap cavity system. Electric-field mode profiles induced by the out-of-plane dipole source at wavelengths of 532 nm with (a) side and (b) top view. Same model at 800 nm is presented in (c, d).*

To understand the enhancement in more details, we carried out FDTD simulations of the plasmonic cavity system. In the model, we assume a linearly polarized light source with 532 nm is incident from top to bottom, emulating the experimental situation. The sideview (top view) of the mode profiles are depicted in **Figure 4a (4b)**, respectively. The excitation enhancement factor is ~ 10 is observed at the mode maximum. To further estimate the enhancement in the radiative decay rates, i.e. Purcell enhancement, an out-of-plane dipole source (λ=800 nm) is placed within the gap. A cross-sectional side and a top view showing the mode induced by the dipole is shown in **Figure 4c** and **4d**, respectively. Note, that these are electric field profiles with dipole emitters with wavelengths of 800 nm. The Purcell factor for the dipole source located at the mode maximum is ~ 200, and calculated

using Lumerical by calculating the dipole power with and without a cavity. The dipole power is defined as the amount of power radiated by the dipole at 800 nm.

To quantify the PL enhancement, we define the average PL enhancement factor across a single cavity as: $\langle EF \rangle = (I_{on} \times A_0)/(I_{off} \times A_{cav})$[43], where Ion is the integrated PL intensity from the IE coupled into the cavity and I_{off} is the PL intensity from IE on bare thermal oxide silicon substrate, A_0 and A_{cav} are the areas of the laser spot and the cavity, respectively. Here we assume that the laser spot is diffraction limited ~$(266nm)^2$ and the cavity size is $(100\ nm)^2$, yielding a maximum <EF> of 106.1 at room temperature and 35.4 and cryogenic temperature, respectively.

To corroborate our experimental results with the simulation values, one can estimate the Purcell enhancement from our experimental data. The small relative lifetime enhancement of 20% at ambient conditions and ~25% at 5K, combined with the simultaneously observed intensity enhancement is indicative that the IEs are dominated by a rather small quantum yield of a few percent, i.e., the experimentally measured lifetime is dominated by non-radiative recombination[44, 45]. For this case, assuming a quantum yield η at the range of ~ 0.5 – 2%, the Purcell enhancement can be expressed as $\eta F_p = (\tau_{free} / \tau_{cav}) - 1$, and is at the range of ~ 12 - 45 in our experiment. Note, that the enhancement measured experimentally corresponds also and to enhancement in the excitation energy as expected for the plasmonic cavity. Note, that this scenario is not unusual, and similar findings are reported for cavity-coupled exciton emission from carbon nanotubes, which display a 20-fold intensity enhancement but only a rather modest lifetime enhancement[46].

Conclusions

To conclude, we have demonstrated the integration of IEs in MoS_2/WS_2 monolayer heterostructures with plasmonic nanocavities. The IEs interacts with the plasmonic cavity modes, leading to a 15-times enhancement in luminescence at room temperature and a 5-times enhancement in PL intensity at cryogenic temperature, respectively. The enhancement of the emission is attributed to the higher absorption efficiency and the Purcell effect from the cavity. Our findings demonstrate a new method to manipulate the excitonic processes in TMD heterojunctions, which is very important for the design of nanophotonic devices from 2D materials.

Materials and Methods

***Samples fabrication*:** A 90 nm thick ultraflat gold film is deposited onto a polished Si substrate using a slow-rate vacuum electron-beam deposition system. The gold surface is coated with a 3 nm thick Al_2O_3 layer using an atomic layer deposition system. Silver nanocubes (side length =100 nm) are purchased from Nanocomplex and the solution is diluted by 100 times using isopropanol prior to use.

Monolayer WS_2, MoS_2 and thin hBN flakes were mechanically exfoliated on silicon substrates with a 300 nm thermal oxide layer. The monolayers and the thickness of hBN flakes were identified firstly with optical microscopy followed by atomic force microscopy and photoluminescence, respectively. The heterostructures were stacked using a poly(vinyl alcohol) stamp based align transfer technique. The stamp was then dissolved with water to release heterostructures onto the gold ultraflat mirror. The silver nanocubes were drop-cast onto the heterostructures prior to optical measurements.

***Photoluminescence spectroscopy*:** The PL spectra were collected with a home-built scanning confocal microscope. The samples were excited with a 200 μW 532nm continuous wave (CW) laser. The reflection signal was spectrally filtered using a 532 nm dichroic mirror (LP03-532RE-25) and a 715 nm long pass filter. The time-correlated PL measurements were performed using the same setup where the samples were excited with a 20 μW 512 nm pulsed laser (PiL051X) with a repetition rate of 20 MHz. The laser signal and the PL from the samples (APD counts) were correlated using a time-correlated single photon counting system (PicoHarp 300). Low-temperatures optical measurements were conducted in the attoDRY800 cryostat.

Scattering spectroscopy: The scattering spectra were done in the manner of dark field imaging in a different home-built confocal microscope at room temperature with a long working distance objective (Nikon CF Plan 50x EPI ELWD) with 0.55 NA. A white light illumination (Thorlabs OSL2) was channelled through a multimode optical fiber and focused onto the sample at an incidence angle of 28° from the surface plane. This low angle of excited light allowed only the scattering light by the silver nanocubes collected by the long working objective.

Acknowledgements

The authors acknowledge financial support from the Australian Research Council (CE200100010) and the Asian Office of Aerospace Research & Development (FA2386-20-1-4014). The authors thank the Australian Nanofabrication Facilities at the UTS OptoFab node.

Conflict of Interest

The authors declare no conflict of interest

References

1. Rivera, P.; Yu, H.; Seyler, K. L.; Wilson, N. P.; Yao, W.; Xu, X., Interlayer valley excitons in heterobilayers of transition metal dichalcogenides. *Nature Nanotech.* **2018,** *13* (11), 1004-1015.

2. Jauregui, L. A.; Joe, A. Y.; Pistunova, K.; Wild, D. S.; High, A. A.; Zhou, Y.; Scuri, G.; De Greve, K.; Sushko, A.; Yu, C.-H.; Taniguchi, T.; Watanabe, K.; Needleman, D. J.; Lukin, M. D.; Park, H.; Kim, P., Electrical control of interlayer exciton dynamics in atomically thin heterostructures. *Science* **2019,** *366* (6467), 870.

3. Liu, Y.; Dini, K.; Tan, Q.; Liew, T.; Novoselov, K. S.; Gao, W., Electrically controllable router of interlayer excitons. *Science Advances* **2020,** *6* (41), eaba1830.

4. Jiang, Y.; Chen, S.; Zheng, W.; Zheng, B.; Pan, A., Interlayer exciton formation, relaxation, and transport in TMD van der Waals heterostructures. *Light: Science & Applications* **2021,** *10* (1), 72.

5. Okada, M.; Kutana, A.; Kureishi, Y.; Kobayashi, Y.; Saito, Y.; Saito, T.; Watanabe, K.; Taniguchi, T.; Gupta, S.; Miyata, Y.; Yakobson, B. I.; Shinohara, H.; Kitaura, R., Direct and Indirect Interlayer Excitons in a van der Waals Heterostructure of hBN/WS2/MoS2/hBN. *ACS Nano* **2018,** *12* (3), 2498-2505.

6. Rivera, P.; Schaibley, J. R.; Jones, A. M.; Ross, J. S.; Wu, S.; Aivazian, G.; Klement, P.; Seyler, K.; Clark, G.; Ghimire, N. J.; Yan, J.; Mandrus, D. G.; Yao, W.; Xu, X., Observation of long-lived interlayer excitons in monolayer MoSe2–WSe2 heterostructures. *Nature Communications* **2015,** *6* (1), 6242.

7. Hanbicki, A. T.; Chuang, H.-J.; Rosenberger, M. R.; Hellberg, C. S.; Sivaram, S. V.; McCreary, K. M.; Mazin, I. I.; Jonker, B. T., Double Indirect Interlayer Exciton in a MoSe2/WSe2 van der Waals Heterostructure. *ACS Nano* **2018,** *12* (5), 4719-4726.

8. Chen, H.; Wen, X.; Zhang, J.; Wu, T.; Gong, Y.; Zhang, X.; Yuan, J.; Yi, C.; Lou, J.; Ajayan, P. M.; Zhuang, W.; Zhang, G.; Zheng, J., Ultrafast formation of interlayer hot excitons in atomically thin MoS2/WS2 heterostructures. *Nature Communications* **2016,** *7* (1), 12512.

9. Merkl, P.; Mooshammer, F.; Steinleitner, P.; Girnghuber, A.; Lin, K. Q.; Nagler, P.; Holler, J.; Schüller, C.; Lupton, J. M.; Korn, T.; Ovesen, S.; Brem, S.; Malic, E.; Huber, R., Ultrafast transition between exciton phases in van der Waals heterostructures. *Nature Materials* **2019,** *18* (7), 691-696.

10. Ovesen, S.; Brem, S.; Linderälv, C.; Kuisma, M.; Korn, T.; Erhart, P.; Selig, M.; Malic, E., Interlayer exciton dynamics in van der Waals heterostructures. *Communications Physics* **2019,** *2* (1), 23.

11. Mueller, T.; Malic, E., Exciton physics and device application of two-dimensional transition metal dichalcogenide semiconductors. *npj 2D Materials and Applications* **2018,** *2* (1), 29.

12. Yuan, L.; Zheng, B.; Kunstmann, J.; Brumme, T.; Kuc, A. B.; Ma, C.; Deng, S.; Blach, D.; Pan, A.; Huang, L., Twist-angle-dependent interlayer exciton diffusion in WS2–WSe2 heterobilayers. *Nature Materials* **2020,** *19* (6), 617-623.

13. Heo, H.; Sung, J. H.; Cha, S.; Jang, B.-G.; Kim, J.-Y.; Jin, G.; Lee, D.; Ahn, J.-H.; Lee, M.-J.; Shim, J. H.; Choi, H.; Jo, M.-H., Interlayer orientation-dependent light absorption and emission in monolayer semiconductor stacks. *Nature Communications* **2015,** *6* (1), 7372.

14. Unuchek, D.; Ciarrocchi, A.; Avsar, A.; Watanabe, K.; Taniguchi, T.; Kis, A., Room-temperature electrical control of exciton flux in a van der Waals heterostructure. *Nature* **2018,** *560* (7718), 340-344.

15. Rivera, P.; Seyler, K. L.; Yu, H.; Schaibley, J. R.; Yan, J.; Mandrus, D. G.; Yao, W.; Xu, X., Valley-polarized exciton dynamics in a 2D semiconductor heterostructure. *Science* **2016,** *351* (6274), 688.

16. Unuchek, D.; Ciarrocchi, A.; Avsar, A.; Sun, Z.; Watanabe, K.; Taniguchi, T.; Kis, A., Valley-polarized exciton currents in a van der Waals heterostructure. *Nature Nanotechnology* **2019,** *14* (12), 1104-1109.

17. Yu, H.; Liu, G.-B.; Tang, J.; Xu, X.; Yao, W., Moiré excitons: From programmable quantum emitter arrays to spin-orbit–coupled artificial lattices. *Science Advances* **2017,** *3* (11), e1701696.

18. Huang, Z.; Liu, Y.; Dini, K.; Tan, Q.; Liu, Z.; Fang, H.; Liu, J.; Liew, T.; Gao, W., Robust Room Temperature Valley Hall Effect of Interlayer Excitons. *Nano Letters* **2020,** *20* (2), 1345-1351.

19. Fang, H.; Battaglia, C.; Carraro, C.; Nemsak, S.; Ozdol, B.; Kang, J. S.; Bechtel, H. A.; Desai, S. B.; Kronast, F.; Unal, A. A.; Conti, G.; Conlon, C.; Palsson, G. K.; Martin, M. C.; Minor, A. M.; Fadley, C. S.; Yablonovitch, E.; Maboudian, R.; Javey, A., Strong interlayer coupling in van der Waals

heterostructures built from single-layer chalcogenides. *Proceedings of the National Academy of Sciences* **2014,** *111* (17), 6198.

20. Chiu, M.-H.; Li, M.-Y.; Zhang, W.; Hsu, W.-T.; Chang, W.-H.; Terrones, M.; Terrones, H.; Li, L.-J., Spectroscopic Signatures for Interlayer Coupling in MoS2–WSe2 van der Waals Stacking. *ACS Nano* **2014,** *8* (9), 9649-9656.

21. Fogler, M. M.; Butov, L. V.; Novoselov, K. S., High-temperature superfluidity with indirect excitons in van der Waals heterostructures. *Nature Communications* **2014,** *5* (1), 4555.

22. Wang, Z.; Rhodes, D. A.; Watanabe, K.; Taniguchi, T.; Hone, J. C.; Shan, J.; Mak, K. F., Evidence of high-temperature exciton condensation in two-dimensional atomic double layers. *Nature* **2019,** *574* (7776), 76-80.

23. Sohoni, M.; Jha, P. K.; Nalabothula, M.; Kumar, A., Interlayer exciton valleytronics in bilayer heterostructures interfaced with a phase gradient metasurface. *Applied Physics Letters* **2020,** *117* (12), 121101.

24. Li, W.; Lu, X.; Dubey, S.; Devenica, L.; Srivastava, A., Dipolar interactions between localized interlayer excitons in van der Waals heterostructures. *Nature Materials* **2020,** *19* (6), 624-629.

25. Qin, J.; Chen, Y.-H.; Zhang, Z.; Zhang, Y.; Blaikie, R. J.; Ding, B.; Qiu, M., Revealing Strong Plasmon-Exciton Coupling between Nanogap Resonators and Two-Dimensional Semiconductors at Ambient Conditions. *Physical Review Letters* **2020,** *124* (6), 063902.

26. Khelifa, R.; Back, P.; Flöry, N.; Nashashibi, S.; Malchow, K.; Taniguchi, T.; Watanabe, K.; Jain, A.; Novotny, L., Coupling Interlayer Excitons to Whispering Gallery Modes in van der Waals Heterostructures. *Nano Letters* **2020,** *20* (8), 6155-6161.

27. Rivera, P.; Fryett, T. K.; Chen, Y.; Liu, C.-H.; Ray, E.; Hatami, F.; Yan, J.; Mandrus, D.; Yao, W.; Majumdar, A.; Xu, X., Coupling of photonic crystal cavity and interlayer exciton in heterobilayer of transition metal dichalcogenides. *2D Materials* **2019,** *7* (1), 015027.

28. Liu, Y.; Fang, H.; Rasmita, A.; Zhou, Y.; Li, J.; Yu, T.; Xiong, Q.; Zheludev, N.; Liu, J.; Gao, W., Room temperature nanocavity laser with interlayer excitons in 2D heterostructures. *Science Advances* **2019,** *5* (4), eaav4506.

29. Yan, J.; Ma, C.; Huang, Y.; Yang, G., Tunable Control of Interlayer Excitons in WS2/MoS2 Heterostructures via Strong Coupling with Enhanced Mie Resonances. *Advanced Science* **2019,** *6* (11), 1802092.

30. Förg, M.; Colombier, L.; Patel, R. K.; Lindlau, J.; Mohite, A. D.; Yamaguchi, H.; Glazov, M. M.; Hunger, D.; Högele, A., Cavity-control of interlayer excitons in van der Waals heterostructures. *Nature Communications* **2019,** *10* (1), 3697.

31. Latini, S.; Ronca, E.; De Giovannini, U.; Hübener, H.; Rubio, A., Cavity Control of Excitons in Two-Dimensional Materials. *Nano Letters* **2019,** *19* (6), 3473-3479.

32. Bogdanov, S. I.; Boltasseva, A.; Shalaev, V. M., Overcoming quantum decoherence with plasmonics. *Science* **2019,** *364* (6440), 532.

33. Hugall, J. T.; Singh, A.; van Hulst, N. F., Plasmonic Cavity Coupling. *ACS Photonics* **2018,** *5* (1), 43-53.

34. Chikkaraddy, R.; de Nijs, B.; Benz, F.; Barrow, S. J.; Scherman, O. A.; Rosta, E.; Demetriadou, A.; Fox, P.; Hess, O.; Baumberg, J. J., Single-molecule strong coupling at room temperature in plasmonic nanocavities. *Nature* **2016,** *535* (7610), 127-130.

35. Kleemann, M.-E.; Chikkaraddy, R.; Alexeev, E. M.; Kos, D.; Carnegie, C.; Deacon, W.; de Pury, A. C.; Große, C.; de Nijs, B.; Mertens, J.; Tartakovskii, A. I.; Baumberg, J. J., Strong-coupling of WSe2 in ultra-compact plasmonic nanocavities at room temperature. *Nature Communications* **2017,** *8* (1), 1296.

36. Rose, A.; Hoang, T. B.; McGuire, F.; Mock, J. J.; Ciracì, C.; Smith, D. R.; Mikkelsen, M. H., Control of Radiative Processes Using Tunable Plasmonic Nanopatch Antennas. *Nano Lett.* **2014,** *14* (8), 4797-4802.

37. Gutiérrez, H. R.; Perea-López, N.; Elías, A. L.; Berkdemir, A.; Wang, B.; Lv, R.; López-Urías, F.; Crespi, V. H.; Terrones, H.; Terrones, M., Extraordinary Room-Temperature Photoluminescence in Triangular WS2 Monolayers. *Nano Lett.* **2013,** *13* (8), 3447-3454.

38. Mak, K. F.; Lee, C.; Hone, J.; Shan, J.; Heinz, T. F., Atomically Thin ${\mathrm{MoS}}_{2}$: A New Direct-Gap Semiconductor. *Physical Review Letters* **2010,** *105* (13), 136805.

39. Wu, K.; Zhong, H.; Guo, Q.; Tang, J.; Zhang, J.; Qian, L.; Shi, Z.; Zhang, C.; Yuan, S.; Zhang, S.; Xu, H., Identification of twist-angle-dependent excitons in WS2/WSe2 heterobilayers. *National Science Review* **2021**.

40. Tongay, S.; Fan, W.; Kang, J.; Park, J.; Koldemir, U.; Suh, J.; Narang, D. S.; Liu, K.; Ji, J.; Li, J.; Sinclair, R.; Wu, J., Tuning Interlayer Coupling in Large-Area Heterostructures with CVD-Grown MoS2 and WS2 Monolayers. *Nano Letters* **2014,** *14* (6), 3185-3190.

41. Li, G.-C.; Zhang, Y.-L.; Jiang, J.; Luo, Y.; Lei, D. Y., Metal-Substrate-Mediated Plasmon Hybridization in a Nanoparticle Dimer for Photoluminescence Line-Width Shrinking and Intensity Enhancement. *ACS Nano* **2017,** *11* (3), 3067-3080.

42. Kim, J.; Jin, C.; Chen, B.; Cai, H.; Zhao, T.; Lee, P.; Kahn, S.; Watanabe, K.; Taniguchi, T.; Tongay, S.; Crommie, M. F.; Wang, F., Observation of ultralong valley lifetime in WSe₂/MoS₂ heterostructures. *Science Advances* **2017,** *3* (7), e1700518.

43. Sun, J.; Hu, H.; Zheng, D.; Zhang, D.; Deng, Q.; Zhang, S.; Xu, H., Light-Emitting Plexciton: Exploiting Plasmon–Exciton Interaction in the Intermediate Coupling Regime. *ACS Nano* **2018,** *12* (10), 10393-10402.

44. Wu, Y.; Xu, J.; Poh, E. T.; Liang, L.; Liu, H.; Yang, J. K. W.; Qiu, C.-W.; Vallée, R. A. L.; Liu, X., Upconversion superburst with sub-2 μs lifetime. *Nature Nanotechnology* **2019,** *14* (12), 1110-1115.

45. Luo, Y.; Shepard, G. D.; Ardelean, J. V.; Rhodes, D. A.; Kim, B.; Barmak, K.; Hone, J. C.; Strauf, S., Deterministic coupling of site-controlled quantum emitters in monolayer WSe2 to plasmonic nanocavities. *Nature Nanotechnology* **2018,** *13* (12), 1137-1142.

46. Jeantet, A.; Chassagneux, Y.; Raynaud, C.; Roussignol, P.; Lauret, J. S.; Besga, B.; Estève, J.; Reichel, J.; Voisin, C., Widely Tunable Single-Photon Source from a Carbon Nanotube in the Purcell Regime. *Phys. Rev. Lett.* **2016,** *116* (24), 247402.

TOC text

In this work we couple interlayer excitons from a heterostructures of tungsten di-sulphide and molybdenum di-sulphide (WS_2/MoS_2) to nanoscale plasmonic gap cavities. Five-fold enhancement is demonstrated, showing the potential for 2D heterostructures for emerging nanophotonic applications